Soft Matter

Cite this: *Soft Matter*, 2011, **7**, 9992

www.rsc.org/softmatter

PAPER

In situ neutron scattering study of structural transitions in fibrin networks under shear deformation

Katie M. Weigandt,[a] Lionel Porcar[bc] and Danilo C. Pozzo*[a]

Received 23rd June 2011, Accepted 5th August 2011
DOI: 10.1039/c1sm06176c

Small angle neutron scattering (SANS) is used to decipher the origin of the strain hardening in biopolymer networks by directly measuring the structural response of a fibrin gel to simple shear deformation. A special Couette shear cell is used to systematically probe the structural properties of a fibrin clot over strain values in the range of $\gamma = 1$–170%. The SANS results indicate that the strain hardening response of coarse fibrin gels occurs in two distinct regions having different structural and mechanical signatures that are separated by an intermediate strain softening regime. At low strains ($\gamma < 10\%$) there is a measurable increase in the shear modulus upon the application of shear strain but there are no significant changes to the clot structure. At higher strain values ($\gamma > 30\%$), a second strain-hardening regime is directly correlated to significant fiber alignment. The mean diameter of the fibers determined directly from two-dimensional fits to the anisotropic scattering data is found to decrease monotonically in the high-strain regime. The results suggest that the non-linear mechanical properties of fibrin clots are the result of a reduction of lateral entropic fluctuations at low strains and a transition between bending and stretching at higher strain values.

Introduction

Fibrinogen is a protein that is naturally present in the blood stream at concentrations of 2–4 mg/mL.[1] Fibrin, the activated form of fibrinogen, is a critical component of blood clots and is primarily responsible for their unique mechanical properties.[2] When tissue is damaged, a cascade of biochemical processes is initiated that leads to the local production of thrombin and subsequently to the cleavage of the amino terminal segments of fibrinopeptides A and B in fibrinogen.[2] This leads to the self-assembly of activated fibrinogen into linear half-staggered structures known as protofibrils. These structures can also aggregate laterally to form thicker fibers and a bifurcating three-dimensional network. The extent of lateral aggregation is determined by a complex balance of local interactions that are affected by solvent properties including ionic strength, pH and the isotopic composition of water.[3–5]

Fibrin gels are highly elastic and exhibit strain dependent non-linear mechanical properties that are unlike those of most synthetic polymer gels. Even at very small protein concentrations (<1 mg mL^{-1}), the fibrin network is very elastic and can effectively support haemostasis at the injury site. It is well accepted that the high elasticity and strain-hardening properties of fibrin are related to the structure of the individual proteins, the fibers, and the network.[6–9] However, the origin of strain-hardening in fibrin and other biopolymers is still not fully resolved and experimental evidence directly linking structural transitions to mechanical properties could provide especially valuable information.[3,6,10]

In a recent paper, it was shown that the linear and non-linear mechanical properties of fibrin gels are highly dependent on deformation and on fibrin concentration.[11] In the same paper it is also demonstrated that neutron scattering is an important tool for the characterization of fully hydrated fibrin gels over multiple relevant length scales (1–10 000 nm). This analysis yielded detailed information about the fibers, their internal structure and the network structure of the gel. The purpose of the current study is to further utilize neutron scattering as a tool to characterize the structure of a fully hydrated fibrin gel *in situ* as it undergoes various degrees of shear deformation. The experimental results of this study are also discussed with respect to recent theoretical models that relate mechanical properties to changes in the gel and the fiber structure.[8,12–17]

The importance of understanding the structural origin of the mechanical behavior of fibrin clots is two-fold. First, fibrin is critical to the restoration of haemostasis and malfunctions in the coagulation process can lead to various disease states.[18] Secondly, purified fibrin is commonly used as a scaffold for tissue growth and as a tissue sealant for surgical applications.[19,20] For these reasons, numerous studies on fibrin mechanics have been reported throughout the literature.[6–8,14,21–23] It is only recently,

[a]*Chemical Engineering Department, University of Washington, Seattle, WA, 98195, USA. E-mail: dpozzo@u.washington.edu*
[b]*Institut Laue-Langevin, Grenoble, France*
[c]*National Institute of Standards and Technology, Gaithersburg, Maryland, USA*

however, that fibrin gels have been characterized in their fully hydrated state over a wide range of concentrations that also extend to values that are relevant to the composition of excised blood clots *in vivo* (>20 mg mL^{-1}).[11,24]

While the microstructure of fibrin gels is largely agreed upon, the origin of strain hardening is still under debate. In the past decade, several theories have emerged to describe the strain stiffening response of biopolymers and to relate this response to the structural features and transitions that occur upon deformation.[13,14,25,26] One important model, emerging from the semi-flexible nature of many natural biopolymers, proposes that a reduction of the conformational entropy in individual stretched fibers leads to an increase of the modulus of the gel upon the application of strain.[13,14,25] On the other hand, an alternative theory for the origin of the strain hardening is based on finite element simulations of discrete fiber networks.[13,26] This model postulates that reduced lateral fluctuations cannot solely explain the high level of strain-hardening that is observed in biopolymer gels including fibrin. It is instead suggested that biopolymer networks undergo strain-hardening primarily as a result of non-affine network rearrangements that govern a transition from the bending of the fibers at crosslinks and bifurcations to the tensile stretching deformation of fibers.[13,26]

Several groups have also sought to expand upon these explanations, or to define the applicability of either model to specific systems.[7,8,15,25,27–29] Kang *et al.* suggest that gels containing coarse fibers are too rigid to undergo entropic strain-hardening and that there is no strain-hardening prior to the alignment of fibers as detected *via* birefringence.[15] Recent work from Brown *et al.* accounted for the high extensibility of fibrin by providing experimental evidence (electron microscopy) that the fibers not only align as they are deformed, but also that the individual proteins unfold.[8,9] Unfolding leads to a measurable reduction in the radius of the protofibril bundle and in the expulsion of water from the individual fibers and the gel as a whole. The authors postulate that this structural transition is also key to the unique mechanical behavior of fibrin. Several other studies link the unfolding of alpha helices within individual protein fibers to their high extensibility and complex mechanical properties.[30,31] The individual fibers are described as having multiple mechanical regimes with a linear response at low deformation that is followed by subsequent softening and then stiffening of the fiber. The softening regime is explained as the unfolding of the alpha helix followed by stiffening as the helix extends to its contour length prior to mechanical failure. Piechocka *et al.* suggest that the extensibility of the fibers results from a reduction in the conformational entropy of the flexible polypeptide chains that facilitate the formation of crosslinks between adjoining protofibrils.[7] This model (loose bundle model) assumes that strain-hardening is purely entropic, but that there is a reduction in lateral fluctuations at both network and inner-fiber scales over two separate strain stiffening regimes.[7] Additionally, very recent work suggests that the extension of the unfolded αC chain between adjoining protofibrils accounts for the high extensibility of strained fibrin gels.[32]

In this work, *in situ* neutron scattering experiments under controlled strain deformations are used to evaluate morphological transitions that occur in fibrin during strain hardening. Through the use of a special Couette shear cell, it is possible to characterize the structure of a clot while finite strains are applied. The shear cell is also unique in that it allows for probing of the deformed sample along the plane defined by the direction of shear strain and the direction of the deformation gradient (a.k.a. 1–2 shear plane).[33] With this cell, the deformation of the network and fiber alignment are directly observed and quantified. The advantages of performing a neutron scattering study are numerous. First, high protein concentrations (>10 mg mL^{-1}) can be used and the resulting data represents a bulk average throughout the sample. In contrast, many optical and microscopic techniques do not penetrate the entire depth of the sample and/or are sometimes restricted to low protein concentrations due to the high turbidity of clots with coarse fibers. Second, by measuring the structure of the strained fibrin *in situ*, we eliminate artifacts that could result from post processing and drying, as well as ensure experimental continuity because measurements at increasing values of strain are obtained from the same gel.

Method

Sample preparation

Human fibrinogen, depleted of plasminogen and von-Willebrand Factor, and human alpha thrombin are purchased from Enzyme Research Laboratories (South Bend, IN). Before use, the fibrinogen is dialyzed over 12 h into a buffer composed of 0.5 mM NaCl, 0.05 mM Tris, 2.5 μM $CaCl_2$ with a pD of 7.4 in D_2O. Several dialysis steps are performed until the resulting protein solution has an isotopic composition of at least 98% deuterium in the solvent. The presence of calcium ions is necessary to activate the enzyme factor XIII that promotes the formation of covalent crosslinks between proteins in the fibers.[34] Before polymerization, the fibrinogen solutions are also degassed under vacuum to prevent the formation of microscopic air bubbles that can affect the scattering signal. Just prior to loading, thrombin is added to the sample at a concentration of 0.16 NIH units per mL and fibrin formation is initiated. All samples are run at a concentration of 10 mg mL^{-1} of fibrinogen.

Neutron scattering

For small angle neutron scattering (SANS), the sample is loaded into a special Couette shear cell that is able to probe the structure of samples under simple shear deformation along the 1–2 shear plane. The technical details of the shear cell have been previously described in the literature.[33] In order to form a fully established clot, the samples are allowed to gel for 10 h prior to mechanical deformation. All neutron scattering experiments are conducted on the NG3 beam line at the NIST Center for Neutron Research in Gaithersburg, MD. For this specific experiment, the instrument is configured with a rectangular sample aperture (1 mm by 3 mm), 8 Å neutron wavelength and a sample to detector distance of 14 m such that the scattering vector, q, is probed between 0.0024 and 0.027 $Å^{-1}$. The sample is sequentially strained to increasing magnitudes by rotating the central shaft of the shear cell (bob). During the scattering experiment, the sample is held at the specified rotation angle while the scattered neutrons are measured. It is determined that a count time of thirty minutes is required to obtain proper statistics with this instrument configuration. The two-dimensional scattering data is reduced to an

absolute scale using the standard NIST Igor procedures.[35] A schematic of the shear cell is shown in Fig. 1 to highlight the direction of the direct beam with respect to the deformation direction.

Rheology

An Anton Paar MCR 301 stress controlled rheometer with a 25 mm cone and plate configuration and a 1° cone angle is used for all rheological measurements. Fibrin gelation is tracked with small amplitude (0.1% strain) oscillations at a frequency of 1 Hz. Strain of this amplitude is well within the linear viscoelastic limit ($\gamma_{LVE} \approx 1\%$) and will not affect the formation of the gel. A 10 h gelation period is necessary to ensure that the extent of crosslinking is consistent between samples and with our previous work so that the properties of the gels are directly comparable.[11] After the gelation period, a fine step-stress ramp is utilized holding each stress for one minute to determine the instantaneous modulus. The strain that is used for the calculation of the modulus is the value measured at the end of each step. Still, it is noted that the covalent crosslinks that occur due to the presence of factor XIII prevent any creep from occurring. To ensure that the sample is not slipping, the strain is monitored as a function of time and the shear stress ramps are also repeated using parallel plate and concentric cylinder geometries. The mechanical properties of the gel are independent of configuration and are free of any slip-induced artifacts.

Results

We previously reported that the non-linear rheology of fibrin gels is highly dependent on both the gel deformation and the initial fibrinogen concentration.[11] In this paper we focus on the structural and mechanical characterization of 10 mg mL^{-1} fibrin gels. These gels have a very distinct rheological signature: they harden, soften and then harden again at increasing levels of deformation.[11] To elucidate the origin of the complex, non-linear mechanical properties of these gels it is necessary to characterize *in situ* the structural properties of a fibrin gel as it is deformed. To this end small angle neutron scattering is used to directly quantify the structural changes that occur as a fully formed fibrin gel is strained.

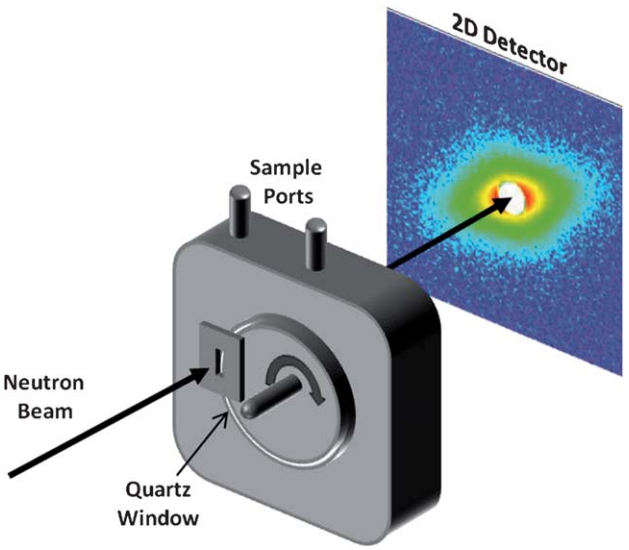

Fig. 1 Schematic of the shear cell with respect to the neutron beam and the two-dimensional detector. Figure is not to scale.

Some of the two-dimensional scattering plots corresponding to specific values of applied shear strain are presented in Fig. 2. In the limit of low strain ($\gamma < 30\%$) the scattering profiles are isotropic indicating that the fibers in the network are randomly oriented. A quantitative analysis of the scattering signal of the unstrained fibrin is found to be in agreement, in terms of the average fiber diameter and the internal fiber structure, with previously reported SANS and USANS measurements.[11] At higher values of strain ($\gamma > 30\%$), the onset of anisotropy in the 2D scattering profiles is characteristic of fiber alignment occurring within the gel. The extent of anisotropy in the scattering is observed to increase with the strain level and the mean fiber alignment direction is also found to be at a finite angle with respect to the shear direction with almost no strain dependence.

In order to quantitatively identify the onset of fiber alignment, an annular average intensity is calculated from the 2D scattering data at each strain as a function of the azimuthal angle, ϕ. This average is performed over a narrow q-range ($0.0045 < q < 0.0054$ Å^{-1}) corresponding to the lowest accessible scattering angles in order to probe the largest possible dimension of the fibers. The annular averages of the scattering intensity at five different strains are shown in Fig. 3. This plot shows that the intensity is only slightly anisotropic at low strains but becomes increasingly anisotropic at strain values greater than $\gamma = 30\%$.

The mean angle of the fiber alignment (ϕ_0), as illustrated in Fig. 3 (right), is obtained directly from the annular average and it is measured relative to the shear direction that is defined as $\phi = 0°$. This parameter only becomes meaningful above $\gamma \sim 30\%$ strain, which is when anisotropy is clearly detectable in the scattering pattern so that the angle can be determined with sufficient certainty. The mean fiber orientation angle ϕ_0 is 34° for γ between 30 and 50%. Above $\gamma = 50\%$, ϕ_0 steadily becomes smaller with increasing strain. Interestingly, the direction of alignment varies weakly as a function of strain. The difference between the orientation angle when the fibers first begin to align ($\gamma \approx 30\%$) and at maximum alignment ($\gamma \approx 170\%$) is just 6°.

In order to further quantify the alignment of the fibers it is necessary to define an orientation distribution function, $F(q, \phi)$. The azimuthally averaged scattering curves are best fit by a Legendre series expansion as in the paper by Burger *et al.*[36] Due to the nature of even Legendre polynomials, it is necessary to apply a phase shift such that the maximum intensity of $I(\phi^*)$ occurs at $\phi^* = 0$. (eqn (1))

$$F(q, \phi^*) = \sum_{n=0}^{\infty} a_n P_{2n}(\cos \phi^*) \quad (1)$$

where $\phi^* = \phi - \left(\phi_0 + \frac{\pi}{2}\right)$, the values, a_n, are fitting coefficients and the functions, P_{2n}, are even Legendre polynomials. We use the first eight terms of the series to fit all of the angular distributions. The resulting fits for several examples are plotted as solid lines in Fig. 3.

From $F(q, \phi)$ we determine the orientation parameter ($\bar{P}_2$) as a function of strain.[36,37] $\bar{P}_2$ is used to quantify the degree of fiber

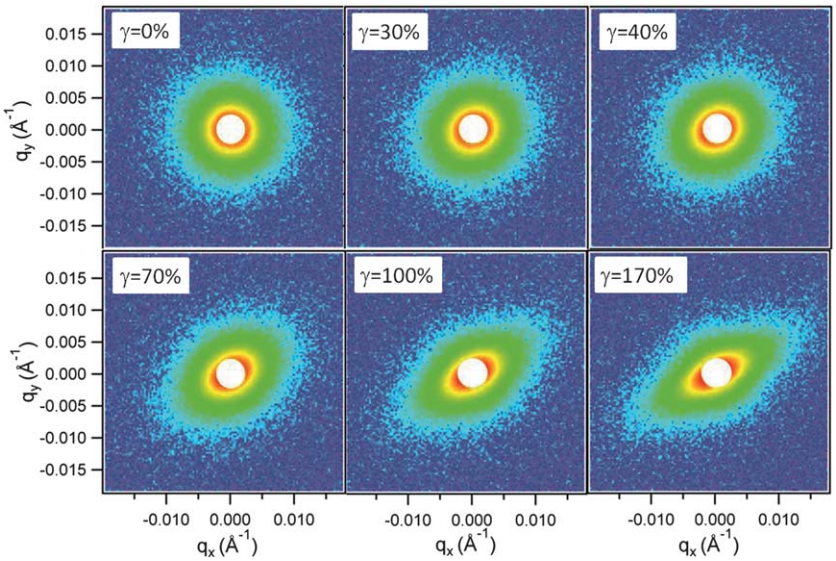

Fig. 2 Reduced two-dimensional neutron scattering data at various strains highlighting the evolution of fibrin structure with increasing strain.

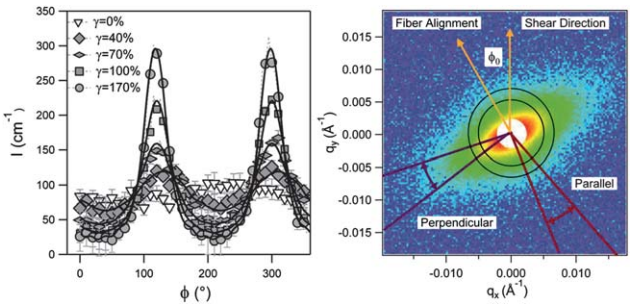

Fig. 3 Left: Annular intensity averages of 2D scattering profiles for 10 mg mL^{-1} fibrin. Lines correspond to the Legendre expansion fits (eqn (1)). Right: Schematic illustrating the definition of ϕ_0, the annulus over which $I(\phi)$ is calculated, and sectors parallel and perpendicular to the direction of fiber alignment for a gel strained to $\gamma = 170\%$. The direction of applied strain (shear direction) is defined as $\phi = 0^\circ$.

alignment in the gel and is directly related to the a_1 coefficient from the Legendre expansion.[36]

$$\overline{P}_2 = \frac{a_1}{5} \tag{2}$$

The value of this orientation parameter will vary between zero for random fiber distribution and one for perfectly aligned fibers. The orientation parameter is calculated for all measured strains. It is found to increase from zero when the gel is unstrained to a maximum value of ~0.35 at the largest strain ($\gamma = 170\%$).

The diameter (D) of the fiber is also determined from the scattering data by fitting to a polydisperse cylinder model. Usually, for randomly oriented objects, the scattering intensity is radially averaged and fitted with a one-dimensional form factor, P(q). For aligned, or partially aligned objects, the scattering intensity, $I(\mathbf{q})$, is anisotropic and is related not only the dimensions of the object, but also to the average particle orientation. In such a case, the traditional methods of analysis such as fitting to an analytical one-dimensional form factor or the use of a cross-sectional Guinier analysis for the determination of fiber radius are no longer valid. Therefore, a two-dimensional model is necessary to quantify the structure (orientation and dimension) of the fibers as a function of strain. This approach is challenging and computationally expensive but, as we will demonstrate, it can provide valuable structural information that is often inaccessible through other techniques. Here, the intensity $I(\mathbf{q})$ at each detector pixel of the two-dimensional scattering profiles for each strain is fit with the 2D cylinder form factor, $P(\mathbf{q})$ (eqn (3)) using SansView:[38]

$$I(\mathbf{q}) = \Phi\pi r^2 L(\Delta\rho)^2 P(\mathbf{q}) + bkg \tag{3}$$

where $\mathbf{q}$ is the scattering vector, Φ is the volume fraction of fibers, r and L are the radius and length of the fibers respectively, $\Delta\rho$ is the scattering length density contrast term, and bkg is the incoherent background. $P(\mathbf{q})$ accounts for the distribution of fiber orientations by averaging the cylinder form factor over the different angular distributions relative to the neutron beam. A detailed description of the two-dimensional cylindrical form factor and the fitting procedures is found in the Supplemental Materials section.

The reduced two-dimensional data and the two-dimensional model fits are shown in Fig. 4 for three characteristic strains. We also compute and show one-dimensional scattering curves using radial averages for isotropic profiles and sector-averages for anisotropic profiles. For aligned samples under strain, the sector averages are taken parallel and perpendicular to the fiber alignment direction ϕ_0 using a sector width of 10°. The quality of the fits is very good considering that every pixel in the detector is being taken into account during fitting. There is a very close match between the one-dimensional scattering curves of the data and the model. The scattering length density of the fiber, which had been allowed to vary during fitting, did not change significantly (<1%) as a function of strain. For the unstrained fibrin clot, we measure a mean diameter of 87 nm that is significantly lower than the values reported in our previous study. This is

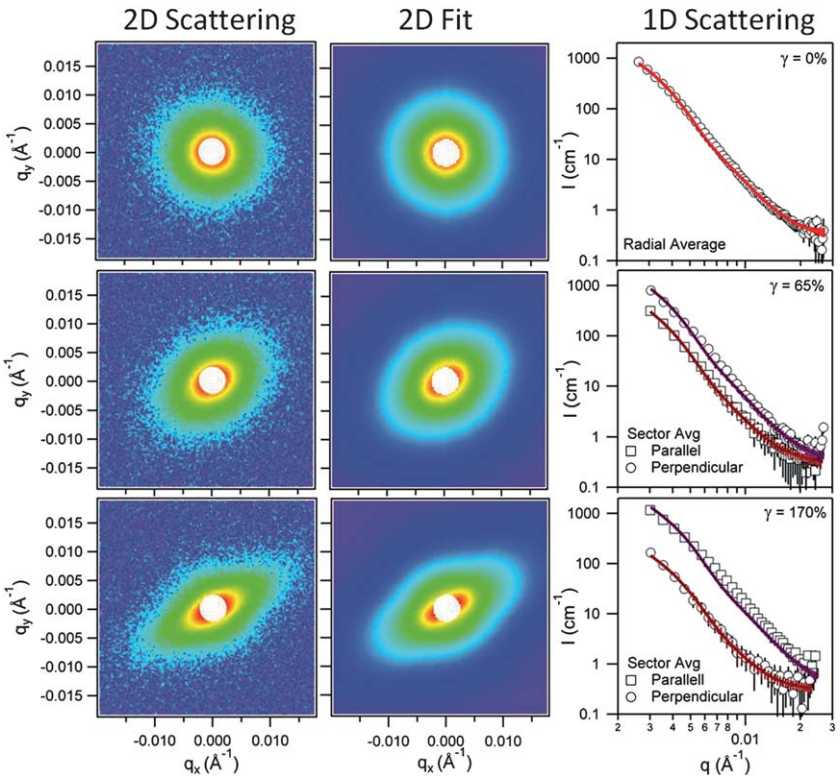

Fig. 4 Two-dimensional scattering data (left), two-dimensional model fits (center), and one-dimensional scattering and fits (right) in the form of sector averages parallel and perpendicular to ϕ_0 for aligned samples or the radial average for the isotropic sample.

because polydispersity in the diameter was accounted for in the 2D model fitting but not in the simple Guinier analysis that was used in our previous paper. The cross-sectional Guinier analysis that is used in the previous report yields a larger diameter because the scattering signal at low angles is more sensitive to the larger fibers. However, when the same cross-sectional Guinier analysis is applied to the unstrained fibrin sample in this study, the resulting diameter is nearly identical to the previously reported value of D ~ 120 nm.[11] Therefore, the structure of the sample has not changed and is comparable to that reported in our previous work. From the fits, we determine that the diameter remains constant until the onset of fiber alignment. At that point, it decreases steadily from 87 nm to 75 nm (14% shrinkage) at the maximum measured strain ($\gamma = 170\%$).

Using identical sample compositions and polymerization conditions, the instantaneous gel modulus (G_{Inst}) is also determined by taking the derivative of the stress as a function of the strain ($d\sigma/d\gamma$) in a separate rheological experiment. The stress and strain are experimentally determined from an applied shear stress ramp using a cone and plate geometry in a stress-controlled rheometer. The modulus is plotted in Fig. 5 as a function of strain. Several key mechanical transitions occur as the gel is strained to $\gamma \sim 30\%$. Even in the low-strain region ($\gamma < 10\%$), the sample undergoes a significant amount of strain-hardening. In this domain, the modulus increases steadily from a rest value of $G_{Inst} = 2300$ Pa to a local maximum of $G_{Inst} = 3400$ Pa at $\gamma = 10\%$. Interestingly, between $\gamma = 10$ and 30% the modulus decreases again to a local minimum of $G_{Inst} = 3000$ Pa. The

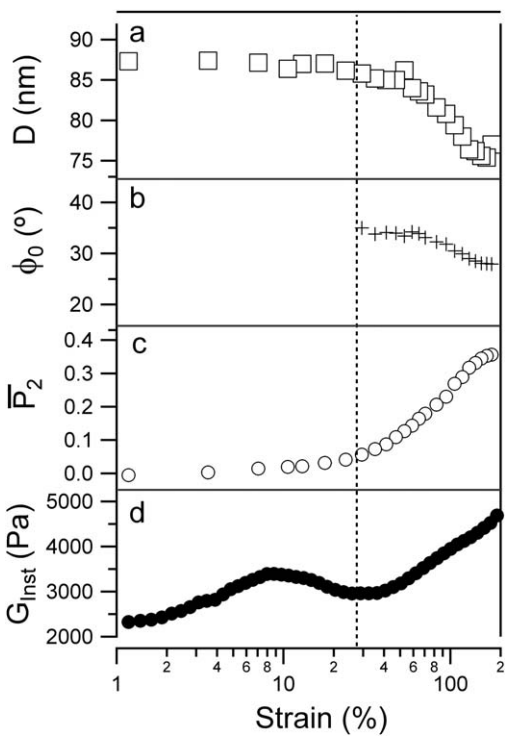

Fig. 5 Fiber diameter (a), fiber alignment angle (b), orientation parameter (c) and instantaneous modulus (d) as a function of applied strain.

scattering data reveals that the average fiber diameter remains relatively unchanged throughout this entire region and that there is no significant fiber alignment (Fig. 5). However, beyond this critical point ($\gamma \sim 30\%$), the average fiber diameter starts to decrease steadily with increasing strain and the fibers begin to align substantially. Note that there is still a clear but small increase in the order parameter at strains less than $\gamma = 30\%$, but the increase in the order parameter occurs much faster once this critical strain has been reached. Finally, a second onset of strain-hardening occurs beyond this critical deformation and there is a clear correlation between the onset of fiber alignment, fiber shrinkage, and strain-hardening. The results presented herein are typical of 10 mg mL^{-1} fibrin gels prepared as detailed in the methods section. Reproducibility of the non-linear rheology is also very good as assessed from systematic experiments. Sometimes there can be variations (<15%) in the absolute magnitude of the instantaneous modulus (G_{Inst}) between different sample loadings but the shape of the curve is always the same. The curves plotted in Fig. 6 are a good demonstration of the reproducibility of the rheology as they include data from two different loadings of the same sample.

At this point, the SANS results cannot fully explain the strain dependent behavior of fibrin gels at strains lower than $\gamma = 30\%$ because there are no measurable changes in the scattering patterns and no structural transitions can be perceived. Still, the instantaneous modulus of a 10 mg mL^{-1} gel shows significant strain dependence between $\gamma = 1$ and 30%. In this region the sample shows a strain-hardening response that is followed by strain-softening. An additional rheological experiment is also performed to further elucidate the nature of the structural changes that occur at low strains ($\gamma < 30\%$). This experiment is based on an examination of the mechanical reversibility of a fibrin gel after sequential stress ramps that are carried out to increasing values of the maximum deformation. Several maximum strain values (γ_{max}) are reached corresponding to regions where key features are observed in the curve of the instantaneous modulus (G_{Inst}). The experiment is performed by gradually straining the gel until it reaches a certain maximum strain (γ_{max}). The deformation is then reversed and the process is repeated to a larger maximum strain value. The instantaneous moduli that are calculated from the stress-strain ramp corresponding to each cycle are plotted in Fig. 6. For comparison, the figure also includes data that is obtained from a separate gel that is deformed directly over the full strain range but using a single continuous ramp.

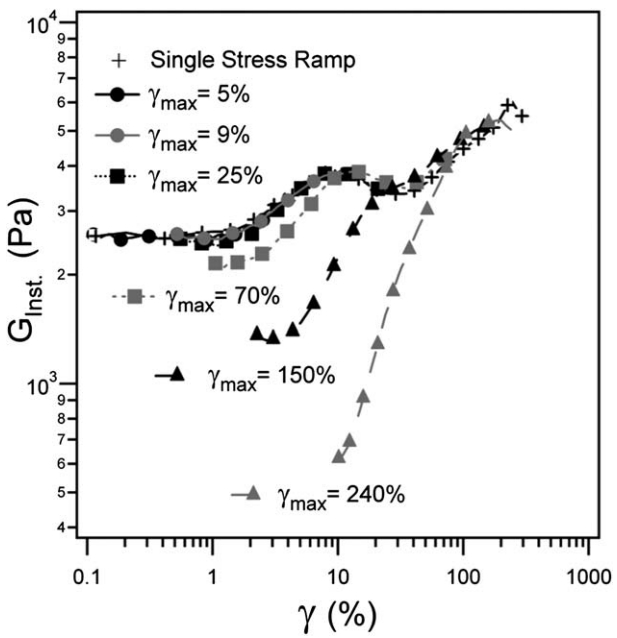

Fig. 6 Instantaneous moduli (G_{Inst}) of a 10 mg mL^{-1} fibrin gel obtained from sequential shear stress ramps with increasing maximum strain γ_{max} values (5%, 9%, 25%, 70%, 150%) until the gel is broken (240%). The instantaneous modulus of a second gel (+), using a single stress ramp until failure, is also shown for comparison.

The instantaneous modulus curves for a gel that is sequentially strained to $\gamma_{max} = 5$, 9 and 25% overlap perfectly. However, on the subsequent strain ramps the instantaneous modulus no longer agrees with the previous cycles at low strain. This indicates that the gel was irreversibly damaged at some point during the last strain ramp, which had reached $\gamma_{max} = 25\%$. Therefore, the limit of reversible deformation in this sample must lie between $\gamma = 9$ and 25%. This suggests that it is only within the first strain-hardening regime that the deformation is completely reversible. The onset of irreversible deformation must lie close to the strain-softening and the second strain-hardening regimes. As the peak strain (γ_{max}) continues to increase in sequential cycles, the low-strain modulus continues to deviate significantly more from that measured in the initial test. This indicates that the clot is experiencing increasing degradation as it is strained to larger and larger levels.

Discussion

Low strain regime ($\gamma < 10\%$)

Fibrin gels have a linear response to deformation only at very small strains ($\gamma < 1\%$). At strains greater than 1% the gel begins to exhibit a non-linear mechanical response that is indicated by an increasing modulus. For moderately low deformation, from $1\% < \gamma < 10\%$, the gel can be described as weakly strain-hardening. That is, the modulus of the gel increases steadily with increasing strain. Furthermore, in this region the deformation of a fibrin gel is fully reversible as shown in Fig. 6. This suggests that no permanent structural damage is done to the gel when it is strained by a low magnitude. Despite the significant increase in modulus that occurs between $\gamma = 1\%$ and $\gamma = 10\%$, the neutron scattering signal remains unchanged at strains of this magnitude. This demonstrates that key structural features of the gel, including fiber diameter and alignment, remain unchanged throughout the first strain-hardening regime. The structure of the gel at low strain is described schematically in Fig. 7.

Of the major theories postulated for explaining strain-hardening in biopolymer gels, it is clear that the bending and stretching model originally proposed by Onck *et al.* requires significant network deformation and alignment of fibers.[26] The absence of alignment in the low strain regime indicates that the bending and stretching model is not an accurate representation of strain-hardening in this gel under small deformation. Conversely, strain-hardening as a result of a reduction in fiber thermal fluctuations will not necessarily have a signature that is

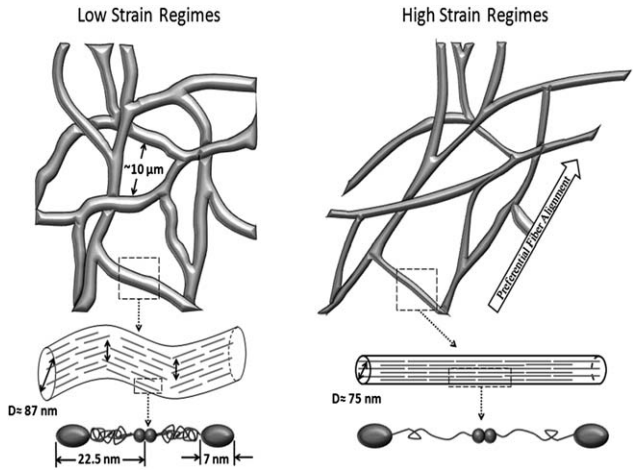

Fig. 7 Schematic description of the various regions that describe the strain-hardening response of fibrin under different levels of deformation.

detectable with small angle neutron scattering. The absence of structural changes corresponding to the first strain-hardening regime suggests that the entropic model is likely the more applicable model for explaining the strain-hardening that is observed in coarse fibrin gels under small deformation. Therefore, even in apparently coarse fibrin gels, the influence of flexibility cannot be fully neglected. A recent report suggests that entropic elasticity can also occur in protofibrils within the individual fibers as a result of lateral fluctuations of the polypeptide chains that facilitate crosslink formation.[7] Furthermore, although the mean fiber diameter that we measure in SANS is relatively large (~87 nm), we still expect that there could be small flexible fibers present that undergo entropic strain-hardening. It should be noted that the scattering signal is biased towards larger structures and this is often reflected in parameters like the mean fiber diameter.[39] Therefore, an alternative explanation is that the low-strain rheology is dominated by the smaller flexible fibers and not by the larger (coarse) fibers that dominate the SANS signal.

Intermediate strain regime (γ = 10–30%)

At intermediate strains (γ = 10–30%) there is a strain-softening regime that separates the two distinct strain-hardening regions. This does not seem to correspond to any significant structural change detectable with neutron scattering over the probed q-range. However, this region does correspond very well with the onset of irreversible deformation (Fig. 6). The fibrin gel is first damaged when it is strained to γ_{max} = 25%, as evidenced by a reduction in the initial instantaneous modulus measured during subsequent deformation cycles. The onset of irreversible deformation, therefore, occurs between 10 and 25% strain. The separation of two strain-hardening regimes by a plateau in the gel modulus was recently reported in the literature.[7,11] In our previous paper we noted that increasing the concentration of fibrin in the gel gradually leads to the development of the strain-softening regime that is also observed in the 10 mg mL^{-1} gel used in this work.[11] The plateau observed in experiments with 8 mg mL^{-1} fibrin samples by other groups is also consistent with this transition.[7] However, they report that the fibrin gel exhibits fully reversible rheology. In contrast, our results indicate that, in a 10 mg mL^{-1} coarse fibrin gel, the deformation is irreversible when the gel is strained beyond the intermediate plateau. In another recent report it was stated that the individual proteins must begin to unfold before the gel is strained above γ = 15% in order to account for the high extensibility of the fibrin gel.[8] This transition is also consistent with the onset of irreversible deformation observed in our study. We expect that the onset of protein unfolding will induce a transition from fully reversible deformation to irreversible deformation as the unfolding of the proteins could irreversibly damage the internal structure of the fibers and protofibrils. Furthermore, several researchers have linked the uncoiling of alpha helices to the softening and subsequent stiffening of individual protein based fibers.[30,31]

To the best of our knowledge none of the previously discussed models is able to predict the intermediate strain-softening behavior that is observed in fibrin gels at high concentrations. Interestingly, a reversible stress-softening response in actin gels was also recently reported.[29] It is postulated that buckling of fibers under compression can lead to a reduction in the number of load-bearing fibers and in an overall reduction in the gel stiffness. This is another plausible mechanism to explain the intermediate strain-softening of fibrin, so further exploration is necessary to fully confirm the origin of this feature.

High strain regime (γ > 30%)

It has been previously suggested that fibrin gels consisting of coarse stiff fibers are better represented by the bending and stretching model.[15] Neutron scattering, as used in this study, is especially suited for testing the validity of models where strain-hardening results from a transition between fiber bending and stretching regimes because they require significant network reorganization. These structural transitions would necessarily result in the alignment of fibrin fibers towards the direction of the applied strain. The progressive alignment of the fibers manifests itself in the neutron scattering measurement as the development of anisotropy, yielding radially-asymmetric scattering patterns. It is evident from Fig. 2–5 that the fibers do align as predicted, but only after a threshold strain of $\gamma \sim$ 30% has been reached. This corresponds well with the onset of the second strain-hardening regime and with the reduction in the average fiber diameter that is shown in Fig. 5.

Recently, it was demonstrated that the application of sufficient stress to coarse fibrin fibers can lead to protein unfolding and the extension of the length of the individual proteins in the fibers.[8] Furthermore, the exposure of hydrophobic residues results in additional bundling of the extended regions and in a net reduction of the average fiber diameter. Our study clearly demonstrates a reduction in fiber diameter that can be attributed to protofibril bundling and also shows that the threshold for bundling occurs simultaneously with the onset of fiber alignment and with the second onset of strain-hardening. The observed fiber alignment and shrinkage is consistent with earlier results.[8] It was previously reported that the fibers begin to align under extensional deformation prior to γ = 50%.[8] In the same study the overall reduction in the fiber diameter that is reported varied from 185 nm at rest, to 74 nm at the maximum deformation

before failure ($\gamma \approx 270\%$). This represents a 250% decrease in fiber diameter upon stretching. In our study, the fibers undergo gradual reduction from 87 to 75 nm that represents a much smaller change of ~14% with respect to the original diameter. The differences in the extent of shrinkage could be partially attributed to a smaller degree of deformation since our study was limited to strains below 200%. It must also be noted that this study uses shear deformation as opposed to extensional deformation. This could also have a significant influence in the extent of fiber alignment and also in the magnitude of fiber contraction. Additionally, these differences could also result from structural changes that are caused by variation in the buffer composition, or changes in the extent of covalent ligation *via* Factor XIII. The structural changes that occur in the high strain regime are also illustrated in Fig. 7.

The 10 mg mL^{-1} coarse fibrin gels examined in this study have two separate strain-hardening regimes, with distinct structural signatures, that are clearly separated by an intermediate reduction of the modulus. These results demonstrate that these gels cannot be solely described with either of the two primary theories for strain-hardening. At low deformations, these gels likely undergo strain-hardening due to a reduction in lateral thermal fluctuations (entropic elasticity).[14] In addition, at larger deformations, the same gels will strain-harden due to a transition from bending-dominated to stretching-dominated mechanical responses.[26] It has also been suggested that, in polydisperse gels containing both fine and coarse fibers, the smaller fibers can exhibit entropic strain-hardening while the response of large fibers is described by bending and stretching models.[15] We propose that it is also possible that both theories are applicable at different levels of deformation. For example, the straightening of individual fibers (rigidification) would likely precede any bending and stretching response. It must be noted that the two models for strain-hardening are not mutually exclusive because they originate from different physical effects.

Conclusions

An experimental framework is developed to simultaneously strain and characterize a fully hydrated biopolymer gel using small angle neutron scattering. Both the fiber dimensions and the extent of alignment are measurable regardless of the opacity of the sample and without any required sample processing steps. The use of neutron scattering enables characterization of structural transitions in a single gel with very fine resolution as a function of strain. In this study, SANS is utilized as a tool to systematically monitor the structure of fibrin gels as a function of increasing strain. This technique proves to be especially useful for determining the structural changes that occur in higher concentration gels as the opacity of these gels prevent the use of most optical techniques. The implementation of two-dimensional form factor fits was critical to the rigorous strain dependent structural characterization of the aligned fibers.[38]

The unique non-linear rheological response of coarse fibrin gels suggests that more than one structural mechanism is responsible for the strain-hardening response in fibrin. We show that both of the primary theories for strain-hardening are necessary to describe the rich rheological behavior of these gels over all levels of deformation. At low strains, a reduction in the conformational entropy of the fibers results in a 50% increase in the shear modulus. This is followed by a region of significant structural changes ($\gamma > 30\%$) where fibers align, stretch and contract radially as shown in Fig. 7. These structural transitions are perfectly correlated with a simultaneous increase in shear modulus of more than 80%. These observations are consistent with a transition from a bending-dominated response to a stretching-dominated region as suggested originally by Onck.[26] Separating these two regions, we find a strain-softening response that is still poorly understood and not fully characterized. Further experiments are necessary to understand the unique strain weakening that occurs at intermediate strains ($10\% < \gamma < 30\%$). Finally, in a very recent paper by Lin and coworkers, a minimalistic model for network mechanics is described.[16] These simple approaches are extremely attractive to describe the mechanical response of networks of rigid fibers from a fundamental thermodynamic framework.

Acknowledgements

We appreciate the efforts of the DANSE team, and in particular Jae Hi Cho, for their implementation and fine tuning of the 2D fitting algorithms in SansView. This work utilized facilities supported in part by the National Science Foundation under Agreement No. DMR-0454672. We acknowledge the support of the National Institute of Standards and Technology, U.S. Department of Commerce, in providing the neutron research facilities used in this work. This work benefited from DANSE software developed under NSF Award DMR-0520547. We also acknowledge the financial support of the University of Washington Royalty Research Fund.

References

1 R. L. Letcher, S. Chien, T. G. Pickering, J. E. Sealey and J. H. Laragh, *Am. J. Med.*, 1981, **70**, 1195–1202.
2 R. F. Doolittle, *Annu. Rev. Biochem.*, 1984, **53**, 195–229.
3 E. A. Ryan, L. F. Mockros, J. W. Weisel and L. Lorand, *Biophys. J.*, 1999, **77**, 2813–2826.
4 U. Larsson, *Eur. J. Biochem.*, 1988, **174**, 139–144.
5 Z. Yang, I. Mochalkin and R. F. Doolittle, *Proc. Natl. Acad. Sci. U. S. A.*, 2000, **97**, 14156–14161.
6 J. P. Collet, H. Shuman, R. E. Ledger, S. T. Lee and J. W. Weisel, *Proc. Natl. Acad. Sci. U. S. A.*, 2005, **102**, 9133–9137.
7 I. K. Piechocka, R. G. Bacabac, M. Potters, F. C. MacKintosh and G. H. Koenderink, *Biophys. J.*, 2010, **98**, 2281–2289.
8 A. E. X. Brown, R. I. Litvinov, D. E. Discher, P. K. Purohit and J. W. Weisel, *Science*, 2009, **325**, 741–744.
9 A. E. X. Brown, R. I. Litvinov, D. E. Discher and J. W. Weisel, 2007.
10 F. C. Mackintosh, J. Kas and P. A. Janmey, *Phys. Rev. Lett.*, 1995, **75**, 4425–4428.
11 K. M. Weigandt, D. C. Pozzo and L. Porcar, *Soft Matter*, 2009, **5**, 4321–4330.
12 P. R. Onck, T. Koeman, T. van Dillen and E. van der Giessen, *Phys. Rev. Lett.*, 2005, **95**.
13 T. van Dillen, P. R. Onck and E. Van der Giessen, *J. Mech. Phys. Solids*, 2008, **56**, 2240–2264.
14 C. Storm, J. J. Pastore, F. C. MacKintosh, T. C. Lubensky and P. A. Janmey, *Nature*, 2005, **435**, 191–194.
15 H. Kang, Q. Wen, P. A. Janmey, J. X. Tang, E. Conti and F. C. MacKintosh, *J. Phys. Chem. B*, 2009, **113**, 3799–3805.
16 D. C. Lin, J. F. Douglas and F. Horkay, *Soft Matter*, 2010, **6**, 3548–3561.
17 A. V. Dobrynin and J. M. Y. Carrillo, *Macromolecules*, 2011, **44**, 140–146.
18 J. W. Weisel, *Biophys. J.*, 1986, **50**, 1079–1093.

19 M. P. Linnes, B. D. Ratner and C. M. Giachelli, *Biomaterials*, 2007, **28**, 5298–5306.
20 S. Basu, C. P. Marini, F. G. Baumann, D. Shirazian, P. Damiani, R. Robertazzi, I. J. Jacobowitz, A. Acinapura and J. N. Cunningham, *Ann. Thorac. Surg.*, 1995, **60**, 1255–1262.
21 C. P. Broedersz, K. E. Kasza, L. M. Jawerth, S. Munster, D. A. Weitz and F. C. MacKintosh, *Soft Matter*, 2010, **6**, 4120–4127.
22 M. Guthold, W. Liu, E. A. Sparks, L. M. Jawerth, L. Peng, M. Falvo, R. Superfine, R. R. Hantgan and S. T. Lord, *Cell Biochem. Biophys.*, 2007, **49**, 165–181.
23 W. Liu, R. Hantgan, J. Mullin, S. Lord, R. Superfine, R. Taylor and M. Guthold, *Biophys. J.*, 2004, **86**, 477A–477A.
24 S. Anand and S. L. Diamond, *Circulation*, 1996, **94**, 763–774.
25 Q. Wen, A. Basu, J. P. Winer, A. Yodh and P. A. Janmey, *New J. Phys.*, 2007, **9**, 428.
26 P. R. Onck, T. Koeman, T. van Dillen and E. van der Giessen, *Phys. Rev. Lett.*, 2005, **95**, 4.
27 N. E. Hudson, J. R. Houser, E. T. O'Brien, R. M. Taylor, R. Superfine, S. T. Lord and M. R. Falvo, *Biophys. J.*, 2010, **98**, 1632–1640.
28 K. A. Erk, K. J. Henderson and K. R. Shull, *Biomacromolecules*, 2010, **11**, 1358–1363.
29 O. Chaudhuri, S. H. Parekh and D. A. Fletcher, *Nature*, 2007, **445**, 295–298.
30 Z. Qin, L. Kreplak and M. J. Buehler, *PLoS One*, 2009, **4**, 14.
31 A. Miserez, S. ScottWasko, C. F. Carpenter and J. H. Waite, *Nat. Mater.*, 2009, **8**, 910–916.
32 J. R. Houser, N. E. Hudson, L. F. Ping, T. O'Brien, R. Superfine, S. T. Lord and M. R. Falvo, *Biophys. J.*, 2010, **99**, 3038–3047.
33 M. W. Liberatore, F. Nettesheim, N. J. Wagner and L. Porcar, *Phys. Rev. E: Stat., Nonlinear, Soft Matter Phys.*, 2006, **73**, 4.
34 J. J. Pisano, J. S. Finlayso and M. P. Peyton, *Science*, 1968, **160**, 892.
35 S. R. Kline, *J. Appl. Crystallogr.*, 2006, **39**, 895–900.
36 C. Burger, B. S. Hsiao and B. Chu, *Polym. Rev.*, 2010, **50**, 91–111.
37 J. J. Hermans, P. H. Hermans, D. Vermaas and A. Weidinger, *Recl. Trav. Chim. Pays-Bas*, 1946, **65**, 427–447.
38 http://danse.chem.utk.edu/sansview.html.
39 O. Spalla, *Neutrons, X-rays, and Light: Scattering Applied to Soft Condensed Matter*, 1st edn, Elsevier, Amsterdam, 2002.

